

Non-linear transport without spin-orbit coupling or warping in two-dimensional Dirac semimetals

Sai Satyam Samal,¹ S. Nandy,² and Kush Saha^{1,3}

¹*National Institute of Science Education and Research, Jatni, Odisha 752050, India*

²*Department of Physics, University of Virginia, Charlottesville, VA 22904, USA*

³*Homi Bhabha National Institute, Training School Complex, Anushakti Nagar, Mumbai 400094, India*

It has been recently realized that the first-order moment of the Berry curvature, namely the *Berry curvature dipole* (BCD) can give rise to non-linear current in a wide variety of time-reversal invariant and non-centrosymmetric materials. While the BCD in two-dimensional Dirac systems is known to be finite only in the presence of either substantial spin-orbit coupling where low-energy Dirac quasiparticles form tilted cones or higher order warping of the Fermi surface, we argue that the low-energy Dirac quasiparticles arising from the merging of a pair of Dirac points without any tilt or warping of the Fermi surface can lead to a non-zero BCD. Remarkably, in such systems, the BCD is found to be independent of Dirac velocity as opposed to the Dirac dispersion with a tilt or warping effects. We further show that the proposed systems can naturally host *helicity*-dependent photocurrent due to their linear momentum-dependent Berry curvatures. Finally, we discuss an important byproduct of this work, i.e., nonlinear anomalous Nernst effect as a second-order thermal response.

Introduction: The Berry phases of electronic wavefunctions can substantially modify the transport properties and give rise to a plethora of anomalous transport phenomena in the linear response regime such as anomalous Hall effect (AHE), anomalous Nernst effect (ANE), quantum charge pumping, etc [1] in systems with broken time-reversal symmetry. Recently, it has also been proposed that the first-order moment of the Berry curvature, namely the Berry curvature dipole (BCD) can give rise to non-linear current in a time-reversal invariant and non-centrosymmetric material [2–4]. Subsequently, the discovery [5, 6] of non-linear anomalous Hall effect (NLAHE) in layered transition metal dichalcogenides (TMDCs) makes the non-linear transport as one of the prime topics of interest to both theorists and experimentalists [2–4, 7–22] in recent times.

Unlike the linear transport properties induced by the Berry curvature, the BCD-induced non-linear transport phenomena such as non-linear anomalous Hall effect, non-linear anomalous Nernst effect (NLANE) and non-linear anomalous thermal Hall effect (NLATHE) is found to be Fermi surface quantities [2, 13, 23, 24]. To find finite values of these non-linear phenomena, one requires either low-symmetry crystals or Dirac Hamiltonian with higher order corrections. For example, it has been shown that the presence of substantial spin-orbit coupling (SOC) where low-energy Dirac quasiparticles form tilted cones is necessary to find a finite NLAHE in two-dimensional (2D) Dirac systems[2]. On the other hand, a recent study [25] showed that the NLAHE can survive in 2D Dirac semimetals even in the absence of complete SOC but with higher order correction to the linearly dispersive Dirac Hamiltonian, particularly with warping of the Fermi surface.

This raises an important question to address, pertinent to several recent and upcoming experiments on 2D

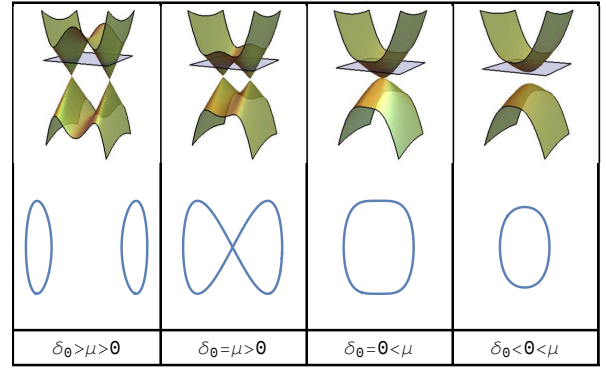


FIG. 1. Evolution of energy spectrum (Eq. 1) (top panel) and corresponding Fermi surface topologies[26] (bottom panel) for different values of parameter δ_0 . For finite chemical potential (μ), the saddle point between the two Dirac nodes evolves with δ_0 and crosses the chemical potential at $\delta_0 = \mu$, leading to topological Lifshitz transition. Note that, for fixed $\delta_0 > 0$, the similar topological transition is obtained by varying μ .

materials: is it possible to realize a finite BCD in a simple low-energy 2D Dirac Hamiltonian *without* any tilting and warping effect. Remarkably, we find that the tilting of the Dirac cone or warping of the Fermi surface is not necessary to observe a non-zero BCD in 2D DSMs. Rather, a simple low-energy Hamiltonian with a pair of Dirac nodes close to each other with a saddle point in between the nodes, or a Dirac system where two Dirac nodes merge with each other at a point turn out to be a simple platform for realizing sizeable BCD-induced non-linear Hall effect. Further, we find that the BCD is independent of Dirac velocity but predominantly depends on the effective mass parameter for a fixed band gap. Moreover, these systems can naturally give rise to *helicity*-dependent photocurrent due to their linear momentum-dependent Berry curvatures, as opposed to the typical

gapped Dirac and semiconducting systems[3]. We finally discuss the contribution of the Berry curvature to the non-linear anomalous Nernst effect.

Deformed graphene with uniaxial stress turns out to be an ideal platform for realizing such model Hamiltonian[27–29]. It has also been argued that TiO₂/VO₂ heterostructures [30, 31] under quantum confinement, (BEDT-TTF)₂I₃ organic salts under pressure [32], photonic metamaterials [33] can be ideal candidate materials to host these types of low energy dispersions. Recent experimental realization of such model Hamiltonian in optical lattices [34] has renewed the quest for materials with tunable Dirac nodes.

Model Hamiltonian: The merging of a pair of Dirac nodes can be modeled by the low-energy Hamiltonian[29, 35]

$$\mathcal{H} = \mathbf{d}(\mathbf{k}) \cdot \boldsymbol{\sigma}, \quad (1)$$

where $\boldsymbol{\sigma}$'s are the Pauli matrices in pseudospin space and $\mathbf{d}(\mathbf{k}) = (\alpha k_x^2 - \delta_0, v k_y, 0)$. Here $\mathbf{k} = (k_x, k_y)$ is the crystal momentum, $\alpha = \hbar^2/2m$ is the inverse of quasiparticle mass along x , v is the Dirac velocity along y , and δ_0 is the parameter which drives the transition between a metallic and insulating phase. For $\delta_0 > 0$, two gapless Dirac nodes are found at $(\pm\sqrt{\delta_0/\alpha}, 0)$. At $\delta_0 = 0$, the two Dirac nodes merge, leading to a special dispersion where electron disperses quadratically along the y direction and linearly along the orthogonal direction. This is typically called semi-Dirac point. For $\delta_0 < 0$, a gapped system with trivial insulating phase is obtained. The corresponding spectrum is shown in Fig. (1). Evidently, the saddle point between the two Dirac nodes evolves with δ_0 , which in turn leads to the topological Lifshitz transition for a fixed chemical potential (μ) (cf. Fig. (1)). Consequently, the area of the Fermi surface (S_F) is found to vary *nonmonotonically* with δ_0 . This is expected to be reflected in the BCD since it is a Fermi surface quantity. We note that for fixed δ_0 , the Lifshitz transition can also be obtained with the variation of μ .

Note that, Eq. 1 obeys effective time-reversal ($\Theta = \mathcal{K}$), particle-hole ($\mathcal{P} = \sigma_y$) and chiral symmetries ($\mathcal{C} = \sigma_y \mathcal{K}$), where \mathcal{K} is the complex conjugation operator. Further, we can define two effective mirror symmetries $M_x : (x, y) \rightarrow (-x, y)$ and $M_y(x, y) : (x, y) \rightarrow (x, -y)$. In momentum space, $M_x = \sigma_0$ and $M_y = \sigma_x$ [36]. It is worth mentioning that Eq. 1 can be effectively obtained from a four band isotropic Dirac Hamiltonian with an anisotropy along x direction[37] without any tilt.

Berry curvature dipole in 2D Dirac semimetals: The simple form of Eq. 1 in terms of fictitious magnetic field $\mathbf{d}(\mathbf{k})$ allows us to write Berry curvature as

$$\Omega^a(\mathbf{k}) = \epsilon_{abc} \frac{1}{2|\mathbf{d}(\mathbf{k})|^3} \mathbf{d}(\mathbf{k}) \cdot \left(\frac{\partial \mathbf{d}(\mathbf{k})}{\partial k_b} \times \frac{\partial \mathbf{d}(\mathbf{k})}{\partial k_c} \right), \quad (2)$$

where ϵ_{abc} is the usual Levi-Civita and $(abc) \in (xyz)$. With this, the Berry curvature dipole as characterized

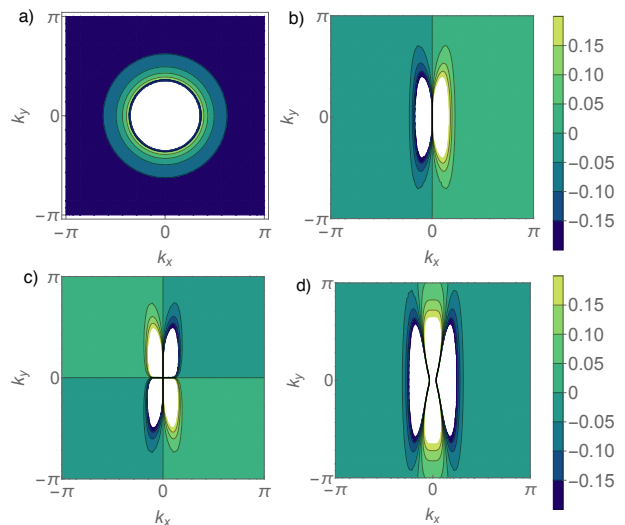


FIG. 2. Top Panel: (a) Contour plot of Berry curvature for isotropic gapped Dirac Hamiltonian. (b) The same plot for the gapped semi-Dirac Hamiltonian discussed in the text. Evidently, $\Omega(-k_x, -k_y) = -\Omega(k_x, k_y)$ as a manifestation of time-reversal symmetry. Lower Panel: (c) and (d) are the contour plots of the derivatives of Ω with respect to k_y and k_x , respectively. Since $\partial_y \Omega(k_x, k_y) = -\partial_y \Omega(k_x, -k_y)$, the integral over k_y at zero temperature is found to be zero, leading to zero Berry curvature dipole along y direction. In contrast, $\partial_x \Omega(k_x, k_y) = \partial_x \Omega(-k_x, k_y)$ which in turn leads to finite Berry dipole. The white spaces in all plots represent very large values of Berry curvatures (peaks or dips in 3D plots).

by the first-order moment of the Berry curvature over the occupied states is defined as

$$D_{ab} = \int_{\mathbf{k}} f_o(\partial_a \Omega_b), \quad (3)$$

where $\int_{\mathbf{k}} = \int d^d k / (2\pi)^d$ and f_o is the Fermi-Dirac distribution function. In three-dimension (3D), the Berry curvature is a pseudovector and consequently, the BCD (D_{ab}) becomes a pseudotensor. On the other hand, in the case of a two-dimensional system, the only nonzero component of the Ω is $\Omega^z(\mathbf{k})$ ($a = z$), indicating the fact that the Berry curvature behaves as a pseudoscalar. Thus in 2D, the pseudotensorial quantity D_{ab} is reduced to a pseudovector quantity (D_a) confined in the 2D plane with only two independent (x and y) components. We point out that for finite Berry curvature dipole to exist, the system must have at most one mirror symmetry left where the single mirror symmetry forces BCD to be orthogonal to the mirror line (i.e. a mirror plane that is perpendicular to the 2D system).

It is easy to see from Eq. (2) that $\Omega(\mathbf{k}) = 0$ for both the bands in Eq. (1) since $d_z = 0$. This is attributed to the fact that Eq. (1) preserves all relevant symmetries protecting the gapless point. To generate finite Berry curvature, we introduce a perturbation $\delta h = m_0 \sigma_z$ to \mathcal{H} , which breaks both \mathcal{P} and M_y symmetry but preserves

Material	m/m_e	m_0 (eV)	μ (eV)	D_x (nm)
(TiO ₂) ₅ /(VO ₂) ₃	13.6	0.2	0.25	0.27
α -(BEDT-TTF) ₂ I ₃	3.1	0.1	0.15	0.86
Photonic crystals	1.2×10^{-3}	1.0	1.5	13.0

TABLE I. Microscopic parameters for semi-Dirac materials, with representative gaps (m_0), chemical potentials, effective masses (m) and corresponding Berry curvature dipoles[30, 33, 38]. Here m_e represents the free electron mass. Evidently, the D_x increases with the decrease in effective band masses as explained in the main text.

M_x and time-reversal symmetry. This gives

$$\Omega(\mathbf{k}) = \frac{\beta k_x}{E_{\mathbf{k}}^3}, \quad (4)$$

where $E_{\mathbf{k}} = \sqrt{|\mathbf{d}(\mathbf{k})|}$ and $\beta = 2\alpha v m_0$. Since $\Omega(\mathbf{k}) = -\Omega(-\mathbf{k})$, the integral of the Berry curvature over the entire Brillouin zone, namely the Chern number turns out to be zero, hence we obtain zero linear anomalous Hall conductivity. It is also apparent from the right top panel of Fig. (2). For comparison, we have also shown Berry curvature for a isotropic Dirac Hamiltonian ($\sigma \cdot \mathbf{k}$) in the left top panel of Fig. (2). Since $\Omega(\mathbf{k}) = \Omega(-\mathbf{k})$, the integral of Ω over the entire Brillouin zone is expected to be finite. However, whether the total Chern number finite or zero depends on the contribution coming from all inequivalent Dirac nodes of the respective lattice model. For example, in graphene, the perturbation δh , namely "Semionoff mass" arising from the staggered on-site potential between two sublattices gives rise to insulting phase as the Chern numbers for the two inequivalent *gapped* Dirac nodes are equal but opposite in sign. We note that such mass term in deformed graphene and other possible candidate materials can be induced by light with different polarization.

At zero temperature, the BCD can be computed using Eq. 3, where the momentum integral is restricted to the region $E_k < \mu$. For the present model, the Fermi surface topology adds complexities in finding the analytical results using Eq. 3. Thus we rewrite Eq. (3) as $D_i = -\int_k v_i \Omega^z f'_0$, where $v_i = \nabla_{k_i} E_{\mathbf{k}}$ with $i \in (x, y)$ and $'$ denotes the derivative with respect to the energy. With this, we obtain

$$\begin{aligned} D_x &= 2 m_0 \sqrt{\alpha} \frac{\sqrt{\mu^2 - m_0^2}}{\mu^3} \mathcal{I}(\mu, \delta_0), \\ D_y &= 0, \end{aligned} \quad (5)$$

where $\mathcal{I}(\mu, \delta_0) = \int_0^{2\pi} d\theta \left(F^+ - F^- \Theta(F^{-2}) \right) |\cos \theta|$ with $F^s = \left(s \sqrt{(\mu^2 - m_0^2)} |\cos \theta| + \delta_0 \right)^{1/2}$, $\Theta(x)$ is the usual Heaviside function. For $\delta_0 = 0$, $\mathcal{I}(\mu, \delta_0)$ can be further

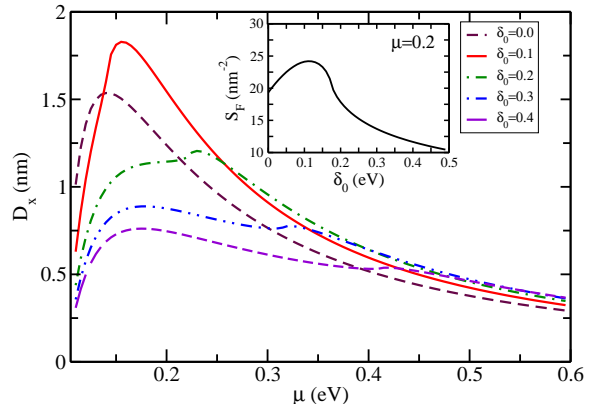


FIG. 3. Berry curvature dipole (BCD) as a function of chemical potential for different values of δ_0 . Clearly for low doping, the BCD increases as the Dirac nodes move close to each other ($\delta_0 \rightarrow 0$). This is attributed to the enhancement of the area of the Fermi surface (S_F) as evident from Fig. (1) and the inset of Fig. 3. However, the Berry dipole suddenly reduces as the two Dirac nodes merge ($\delta_0 = 0.0$) into a single one, corroborating the nonmonotonic nature of the S_F (see inset). For high doping, the S_F does not change substantially with δ_0 , leading to similar D_x . Here, we have used $m_0 = 0.1$ eV and $m/m_e = 13.6$ for (TiO₂)₅/(VO₂)₃.

simplified and Eq. 5 reads off

$$D_x = 2 m_0 \sqrt{\alpha} \mathcal{I}_0 \frac{(\mu^2 - m_0^2)^{3/4}}{\mu^3}, \quad (6)$$

where $\mathcal{I}_0 \simeq 3.5$. To obtain Eq. (5), we have used the parametrization $k_x = \text{sign}[\cos \theta] \left(\frac{r |\cos \theta| + \delta_0}{\alpha} \right)^{1/2}$ and $k_y = \frac{r \sin \theta}{v}$ [39]. Note that the Berry curvature dipole along x survives due to the surviving mirror symmetry M_x while $D_y = 0$ as a consequence of broken M_y . Moreover, D_x vanishes if μ lies inside the bulk gap i.e. $\mu \leq m_0$. Notice that D_x is independent of Dirac velocity v , which is in sharp contrast to the BCD for typical Dirac dispersion with a tilt or warping terms[2, 25]. Also, it is indeed apparent that for materials with small band gap and small effective mass, the BCD is expected to be very large. In Table I, we have presented typical mass parameters with representative gaps and corresponding Berry curvature dipoles for proposed semi-Dirac materials. Evidently, the BCD in a semi-Dirac material is comparable or larger than the BCD in materials with tilting such as SnTe ($D \sim 3$ nm), TMDCs ($D \sim 10^{-2}$ nm)[2] or materials with warping such as graphene ($D \sim 10^{-3}$ nm)[25].

Figure 3 demonstrates the Berry curvature dipole with the variation of δ_0 . For low doping, D_x increases as δ_0 decreases. However, at $\delta_0 = 0$, the D_x suddenly reduces compared to the D_x at $\delta_0 > 0$ as apparent from the

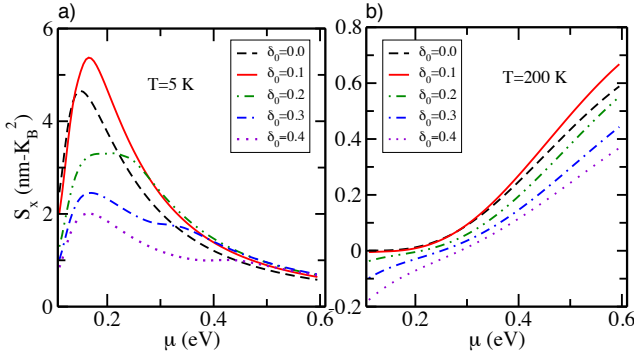


FIG. 4. a) Nonlinear Nernst coefficient (S_x) as a function of chemical potential (μ) for different values of δ_0 . It is apparent that S_x mimics the D_x even in the presence of additional term $(E_k - \mu)^2$ at low temperature ($T=5$ K). b) The same plot for $T=200$ K. All parameters are used same as Fig. 3.

Fig. (3). This is because the area of the Fermi surface, S_F changes *nonmonotonically* with δ_0 as illustrated in the inset of Fig. (3). This behavior can further be understood from the Fig. (1). For finite μ in the conduction band, we have a single Fermi surface at $\delta_0 = 0$ since the band has only one minima (refers to semi-Dirac node). As we move away from $\delta_0 = 0$, the single minima splits into two minimas (refers to Dirac nodes) and a saddle point appears between them. However, the single Fermi surface retains as long as $\delta_0 < \sqrt{\mu^2 - m_0^2}$. Accordingly, the area increases due to the additional curvature arising from the splitting of the single minima. As we further increase δ_0 , the saddle point crosses μ at $\delta_0 = \sqrt{\mu^2 - m_0^2}$, leading to two Fermi surfaces. Consequently, the area starts to decrease. If we increase δ_0 even more, the bands near the Dirac nodes become narrower, which results in the reduction of S_F . For high doping, the Fermi surface topology almost remains same irrespective of the values of δ_0 , leading to similar D_x . Note that this feature of BCD differs from the case for fixed δ_0 but varying chemical potential where S_F monotonically increases with μ (not shown here). We also note that the BCD is found to have a little kink at $\mu = \sqrt{\delta_0^2 + m_0^2}$ as a manifestation of topological Lifshitz transition.

Non-linear photo current: We next move to the Berry curvature contribution to the dc photocurrent. In the presence of an external electric field ($\mathcal{E}e^{i\omega t}$) with $\mathcal{E} \in \mathbb{C}$, the non-linear current is produced due to the Berry phase of Bloch electrons. In particular, the anomalous velocity of the Bloch electrons gives rise to a net current:

$$\mathbf{j} = e \int_{\mathbf{k}} \left[\dot{\mathbf{k}} \times \boldsymbol{\Omega}(\mathbf{k}) \right] f_{neq}(\mathbf{k}), \quad (7)$$

where $f_{neq}(\mathbf{k})$ is the non-equilibrium electron distribution function and $\dot{\mathbf{k}} = \text{Re}(\frac{e}{\hbar} \mathcal{E} e^{i\omega t})$. In the relaxation time approximation with energy-independent scattering time τ , the non-equilibrium electron distribution is ob-

tained to be[3]

$$f_{neq}(\mathbf{k}) = 2\tau e f_0' \frac{(\text{Re } \mathcal{E} - \omega \tau \text{Im } \mathcal{E}) \cdot v}{1 + \omega^2 \tau^2} \quad (8)$$

Assuming low temperature and low frequency, Eq. (7) together with Eq. (8) leads to

$$\mathbf{j} = \frac{\chi}{1 + \omega^2 \tau^2} \left[\frac{1}{\tau} [\mathcal{E}_y \mathcal{E}_x^*]_+ \hat{x} + i\omega [\mathcal{E}_y \mathcal{E}_x^*]_- \hat{x} - \frac{2}{\tau} |\mathcal{E}_x|^2 \hat{y} \right], \quad (9)$$

where $[AB^*]_{\pm} = AB^* \pm A^*B$ and χ is obtained to be

$$\chi = \frac{e^3}{\hbar} \int \frac{d^2 k}{2\pi} v_x \Omega^z(\mathbf{k}) \delta(\mu - E_{\mathbf{k}}) = \frac{e^3}{\hbar} D_x. \quad (10)$$

The first two terms in Eq. (9) are known as linear (LPGE) and circular (CPGE) photogalvanic currents, respectively. The last term in Eq. (9) denotes typical photovoltaic effect. It is clear that the CPGE changes sign with the helicity of the light wave and it is maximum for circularly polarized light. In contrast, the LPGE is dominant and maximum for linearly polarized light. We further see that the non-linear conductivity is nothing but the Berry curvature dipole, corroborating the relation between photocurrent and Berry dipole as expected[2]. For a laser power of 1 Watt, $\omega \tau = 1$, $m = 13.6m_e$ ($(\text{TiO}_2)_5/(\text{VO}_2)_3$), the current density is found to be roughly of the order of 300 nA/mm , which can be easily measured in standard experiments.

To this end, we note that the anomalous velocity associated with the Berry curvature gives rise to helicity-dependent photocurrent if $\Omega(\mathbf{k}) \propto \mathbf{k}$ as pointed out in Ref. [3]. It has been shown that while the Berry phase contribution vanishes in the bulk of a semiconductor quantum well, the surface confinement leads to the helicity-dependent photocurrent due to the particular nature of the Berry curvature. Interesting, our present model naturally gives rise to the helicity-dependent photocurrent without any external perturbation as $\Omega = \beta k_x / E_{\mathbf{k}}^3$ (cf. Eq. 4), in contrast to the typical Dirac dispersion.

Non-linear Anomalous Nernst Effect: Next, we turn to non-linear anomalous Nernst effect in this system. Using the semiclassical Boltzmann theory within the relaxation time approximation, the non-linear anomalous Nernst coefficient at temperature (T) can be defined as [13, 23]

$$S_i = \int_{\mathbf{k}} \frac{(E_{\mathbf{k}} - \mu)^2}{T^2} v_i \Omega(\mathbf{k}) f_0'. \quad (11)$$

The NLANE (second-order response function to the applied temperature gradient), which refers to the nonlinear current, flowing perpendicular to the temperature gradient even in the absence of a magnetic field, is induced by the BCD and therefore, only x -component of it i.e., S_x is finite in this system. In Fig. (4), we show the behavior

of Nernst coefficient at two different temperatures $T = 5$ K and $T = 200$ K. The qualitative feature turns to be same as BCD at low temperature even in the presence of the additional term $(E_K - \mu)^2$ in Eq. (11). However, at high temperature it deviates substantially from the low temperature behavior as evident from Fig. (4). Notice that in both cases, the non-monotonicity of the area of the Fermi surface as discussed before is reflected.

Conclusion: To conclude, we have identified a simple platform to observe substantial non-linear transport phenomena arising from the Berry curvature dipole (BCD). Specifically, we have shown that the sizable BCD can be obtained in a low-energy Dirac Hamiltonian with two Dirac nodes close to each other or their merging at a single node, namely the semi-Dirac node. Remarkably, the BCD for the present model is found to be independent of the Dirac velocity and predominantly depends on the inverse of effective mass of the Dirac quasiparticles as compared to the typical isotropic Dirac systems with well separated Dirac nodes. Indeed, this is one of the interesting findings of this study. For typical Dirac materials, v is of the order of $10^5 m/s$ and does not vary significantly from one material to another. However, the effective masses may vary significantly as evident from the Table I of possible semi-Dirac systems. This fact may guide us to identify materials with low effective masses responsible for a sizable BCD than the only velocity dependent BCD. For example, the candidate semi-Dirac materials have very low effective masses (Table I), hence they are potential platforms to observe BCD-induced large non-linear transport phenomena. We further show that the present model naturally host the helicity-dependent photocurrent due to the linear momentum-dependent Berry curvature in contrast to the isotropic Dirac dispersion. Finally, we present non-linear Nernst effect, arising solely due to the Berry curvature effect. Since the NLAHE can transform ac electric fields into dc currents, a process known as rectification[40], the proposed Dirac materials may have great potential applications for next-generation wireless and energy-harvesting devices.

Acknowledgement: KS is thankful to A. Jaiswal for useful discussion.

[1] D. Xiao, M.-C. Chang, and Q. Niu, Berry phase effects on electronic properties, *Rev. Mod. Phys.* **82**, 1959 (2010).
 [2] I. Sodemann and L. Fu, Quantum nonlinear hall effect induced by berry curvature dipole in time-reversal invariant materials, *Phys. Rev. Lett.* **115**, 216806 (2015).
 [3] J. E. Moore and J. Orenstein, Confinement-induced berry phase and helicity-dependent photocurrents, *Phys. Rev. Lett.* **105**, 026805 (2010).
 [4] T. Low, Y. Jiang, and F. Guinea, Topological currents in black phosphorus with broken inversion symmetry, *Phys. Rev. B* **92**, 235447 (2015).

[5] Q. Ma, S.-Y. Xu, H. Shen, D. MacNeill, V. Fatemi, T.-R. Chang, A. M. Mier Valdivia, S. Wu, Z. Du, C.-H. Hsu, S. Fang, Q. D. Gibson, K. Watanabe, T. Taniguchi, R. J. Cava, E. Kaxiras, H.-Z. Lu, H. Lin, L. Fu, N. Gedik, and P. Jarillo-Herrero, Observation of the nonlinear hall effect under time-reversal-symmetric conditions, *Nature* **565**, 337 (2019).
 [6] K. Kang, T. Li, E. Sohn, J. Shan, and K. F. Mak, Nonlinear anomalous hall effect in few-layer wte2, *Nature Materials* **18**, 324 (2019).
 [7] J. Son, K.-H. Kim, Y. H. Ahn, H.-W. Lee, and J. Lee, Strain engineering of the berry curvature dipole and valley magnetization in monolayer mos₂, *Phys. Rev. Lett.* **123**, 036806 (2019).
 [8] Y. Zhang, Y. Sun, and B. Yan, Berry curvature dipole in weyl semimetal materials: An ab initio study, *Phys. Rev. B* **97**, 041101 (2018).
 [9] J.-S. You, S. Fang, S.-Y. Xu, E. Kaxiras, and T. Low, Berry curvature dipole current in the transition metal dichalcogenides family, *Phys. Rev. B* **98**, 121109 (2018).
 [10] Z. Z. Du, C. M. Wang, H.-Z. Lu, and X. C. Xie, Band signatures for strong nonlinear hall effect in bilayer wte₂, *Phys. Rev. Lett.* **121**, 266601 (2018).
 [11] C. Xiao, Z. Z. Du, and Q. Niu, Theory of nonlinear hall effects: Modified semiclassics from quantum kinetics, *Phys. Rev. B* **100**, 165422 (2019).
 [12] S. Nandy and I. Sodemann, Symmetry and quantum kinetics of the nonlinear hall effect, *Phys. Rev. B* **100**, 195117 (2019).
 [13] C. Zeng, S. Nandy, A. Taraphder, and S. Tewari, Nonlinear nernst effect in bilayer wte₂, *Phys. Rev. B* **100**, 245102 (2019).
 [14] O. Matsyshyn and I. Sodemann, Nonlinear hall acceleration and the quantum rectification sum rule, *Phys. Rev. Lett.* **123**, 246602 (2019).
 [15] B. T. Zhou, C.-P. Zhang, and K. Law, Highly tunable nonlinear hall effects induced by spin-orbit couplings in strained polar transition-metal dichalcogenides, *Phys. Rev. Applied* **13**, 024053 (2020).
 [16] D.-F. Shao, S.-H. Zhang, G. Gurung, W. Yang, and E. Y. Tsymlal, Nonlinear anomalous hall effect for néel vector detection, *Phys. Rev. Lett.* **124**, 067203 (2020).
 [17] Z. Z. Du, C. M. Wang, S. Li, H.-Z. Lu, and X. C. Xie, Disorder-induced nonlinear hall effect with time-reversal symmetry, *Nature Communications* **10**, 3047 (2019).
 [18] H. Wang and X. Qian, Ferroelectric nonlinear anomalous hall effect in few-layer wte₂, *npj Computational Materials* **5**, 119 (2019).
 [19] Z. Z. Du, C. M. Wang, H.-P. Sun, H.-Z. Lu, and X. C. Xie, Quantum theory of the nonlinear hall effect (2020), [arXiv:2004.09742 \[cond-mat.mes-hall\]](https://arxiv.org/abs/2004.09742).
 [20] Y. Zhang, J. van den Brink, C. Felser, and B. Yan, Electrically tuneable nonlinear anomalous hall effect in two-dimensional transition-metal dichalcogenides WTe 2 and MoTe 2, *2D Materials* **5**, 044001 (2018).
 [21] J. I. Facio, D. Efremov, K. Koepf, J.-S. You, I. Sodemann, and J. van den Brink, Strongly enhanced berry dipole at topological phase transitions in bitei, *Phys. Rev. Lett.* **121**, 246403 (2018).
 [22] H. Rostami and V. Juričić, Probing quantum criticality using nonlinear hall effect in a metallic dirac system, *Phys. Rev. Research* **2**, 013069 (2020).
 [23] X.-Q. Yu, Z.-G. Zhu, J.-S. You, T. Low, and G. Su, Topological nonlinear anomalous nernst effect in strained tran-

- sition metal dichalcogenides, *Phys. Rev. B* **99**, 201410 (2019).
- [24] C. Zeng, S. Nandy, and S. Tewari, Wiedemann-franz law and mott relation for non-linear anomalous transport phenomena (2019), [arXiv:1909.03047](https://arxiv.org/abs/1909.03047) [cond-mat.mes-hall].
- [25] R. Battilomo, N. Scopigno, and C. Ortix, Berry curvature dipole in strained graphene: A fermi surface warping effect, *Phys. Rev. Lett.* **123**, 196403 (2019).
- [26] The Fermi surface topologies represent here an equation of a contour satisfying $E(k_x, k_y) = \mu$, where $E(k_x, k_y)$ is the energy spectrum of the conduction band.
- [27] M. O. Goerbig, J.-N. Fuchs, G. Montambaux, and F. Piéchon, Tilted anisotropic dirac cones in quinoid-type graphene and α -(BEDT-TTF)₂I₃, *Phys. Rev. B* **78**, 045415 (2008).
- [28] P. Dietl, F. Piéchon, and G. Montambaux, New magnetic field dependence of landau levels in a graphenelike structure, *Phys. Rev. Lett.* **100**, 236405 (2008).
- [29] Montambaux, G., Piéchon, F., Fuchs, J.-N., and Goerbig, M. O., A universal hamiltonian for motion and merging of dirac points in a two-dimensional crystal, *Eur. Phys. J. B* **72**, 509 (2009).
- [30] V. Pardo and W. E. Pickett, Half-metallic semi-dirac-point generated by quantum confinement in tio₂/vo₂ nanostructures, *Phys. Rev. Lett.* **102**, 166803 (2009).
- [31] G. Montambaux, F. Piéchon, J.-N. Fuchs, and M. O. Goerbig, Merging of dirac points in a two-dimensional crystal, *Phys. Rev. B* **80**, 153412 (2009).
- [32] S. Katayama, A. Kobayashi, and Y. Suzumura, ressure-induced zero-gap semiconducting state in organic conductor α -(bedt-ttf)₂i₃ salt, *J. Phys. Soc. Jpn.* **75**, 054705 (2006).
- [33] Y. Wu, A semi-dirac point and an electromagnetic topological transition in a dielectric photonic crystal, *Opt. Express* **22**, 1906 (2014).
- [34] L. Tarruell, D. Greif, T. Uehlinger, G. Jotzu, and T. Esslinger, Creating, moving and merging dirac points with a fermi gas in a tunable honeycomb lattice, *Nature* **483**, 10871 (2012).
- [35] P. Adrogue, D. Carpentier, G. Montambaux, and E. Orignac, Diffusion of dirac fermions across a topological merging transition in two dimensions, *Phys. Rev. B* **93**, 125113 (2016).
- [36] J. Kim, S. S. Baik, S. W. Jung, Y. Sohn, S. H. Ryu, H. J. Choi, B.-J. Yang, and K. S. Kim, Two-dimensional dirac fermions protected by space-time inversion symmetry in black phosphorus, *Phys. Rev. Lett.* **119**, 226801 (2017).
- [37] F. Peña Benitez, K. Saha, and P. Surówka, Berry curvature and hall viscosities in an anisotropic dirac semimetal, *Phys. Rev. B* **99**, 045141 (2019).
- [38] M. G. Kaplunov, E. B. Yagubskii, L. P. Rosenberg, and Y. G. Borodko, Optical properties of the two crystal modifications of the organic conductor (bedt-ttf)₂i₃, *physica status solidi (a)* **89**, 509.
- [39] I. Mandal and K. Saha, Thermopower in an anisotropic two-dimensional weyl semimetal, *Phys. Rev. B* **101**, 045101 (2020).
- [40] H. Isobe, S.-Y. Xu, and L. Fu, High-frequency rectification via chiral bloch electrons, *Science Advances* **6**, 10.1126/sciadv.aay2497 (2020).